Title
Evidence of complement dysregulation in outer retina of Stargardt disease donor eyes

Authors
Hu, Jane
Pauer, Gayle J
Hagstrom, Stephanie A
et al.

Publication Date
2020-10-01

DOI
10.1016/j.redox.2020.101787

Peer reviewed

Redox Biology 37 (2020) 101787

Contents lists available at ScienceDirect

Redox Biology

journal homepage: www.elsevier.com/locate/redox

Research Paper

Evidence of complement dysregulation in outer retina of Stargardt disease donor eyes

Jane Hu [a], Gayle J. Pauer [b], Stephanie A. Hagstrom [b,c], Dean Bok [a], Meghan J. DeBenedictis [b], Vera L. Bonilha [b,c], Joe G. Hollyfield [b,c], Roxana A. Radu [a,*]

[a] UCLA Stein Eye Institute and Department of Ophthalmology, David Geffen School of Medicine at University of California at Los Angeles, Los Angeles, CA, 90095, USA
[b] Department of Ophthalmic Research, Cole Eye Institute, Cleveland Clinic, 9500 Euclid Avenue, Cleveland, OH, 44195, USA
[c] Department of Ophthalmology, Cleveland Clinic Lerner College of Medicine of Case Western Reserve University, Cleveland, OH, 44195, USA

ARTICLE INFO

Keywords:
Stargardt disease
Complement system
Retinal pigment epithelium
Membrane attack complex
Bisretinoid-lipofuscin
Age-related macular degeneration

ABSTRACT

Stargardt macular degeneration (STGD) is a central blinding disease caused by loss of or dysfunctional ABCA4 transporter in both photoreceptors and retinal pigment epithelial (RPE) cells. Toxic bisretinoid-lipofuscin buildup in the RPE cells is a pathological hallmark of STGD patients and its mouse model, the *Abca4*$^{-/-}$. These vitamin A-derived fluorophores have been shown to induce oxidative stress, stimulate complement activity, and cause chronic inflammation of the RPE. In vivo modulation of complement regulatory pathway in the STGD mouse model has partially rescued the STGD phenotype suggesting that complement attack on the RPE is an important etiologic factor in disease pathogenesis. While bisretinoid-dependent complement activation was further evidenced in cultured RPE cells, this pathway has never been investigated directly in the context of RPE from STGD donor eyes. In the current study, we evaluate the complement reactivity in postmortem donor eyes of clinically diagnosed STGD patients. All three STGD donor eyes RPE displayed strong immunoreactivity for an antibody specific to 4-Hydroxynonenal, a lipid peroxidation byproduct. Also, unlike the control eyes, all three STGD donor eyes showed significantly increased membrane attack complex deposition on the RPE cells. In STGD eyes, increased MAC accumulation was mirrored by elevated C3 fragments internalized by the RPE and inversely correlated with the levels of complement factor H, a major complement regulatory protein. Here, we report the first direct evidence of RPE complement dysregulation as a causative factor in developing Stargardt phenotype.

1. Introduction

Stargardt macular dystrophy (STGD) is a central blinding disease caused primarily by mutations in the *ABCA4* gene [1,2]. Mutations in the *ABCA4* translate into defective or null ABCA4 protein, an ATP binding cassette transporter, that lead to STGD phenotype, including massive number of autofluorescent lipofuscin granules in the retinal pigment epithelium (RPE) and loss of the photoreceptor cells [3]. Recently, our group showed that the protein encoded by the *ABCA4* gene is endogenously made by the RPE cells in addition to the photoreceptor cells [4]. Irrespective of cellular localization, the ABCA4 transporter facilitates the clearance of free retinaldehyde across the photoreceptor outer-segment (OS) disc membranes and RPE endolysosomal membranes respectively to prevent bisretinoid formation [4,5]. As a consequence of a dysfunctional ABCA4 transporter, dimers of vitamin A build up within the lipofuscin granules in RPE cells. Autofluorescent lipofuscin deposits precede photoreceptor cell death and visual loss in STGD patients [6,7]. One major fluorophore of lipofuscin is the retinaldehyde-dimer, *N*-retinylidene-*N*-retinylethanolamine (A2E). In *Abca4*$^{-/-}$ mice, the A2E-bisretinoid level is dramatically increased over time and its rate of accumulation is significantly higher compared to the age-matched wild-type mice [8]. This fluorescent metabolite accumulation is also greatly increased in STGD patients [9]. Bisretinoids and their oxidation products, both constituents of lipofuscin, exhibit several mechanisms of cytotoxicity [10–13] and are thought to contribute to STGD pathogenesis [14]. Specifically, the bisretinoids and

Abbreviations: BrM, Bruch's Membrane; C3b, C3 complement fragment; CC, Choroid capillaries; L, Lipofuscin; ML, Melanolipofuscin; MV, Microvilli; N, Nucleus; STGD, Stargardt disease; TJ, Tight junctions.

* Corresponding author. UCLA Stein Eye Institute, Department of Ophthalmology, David Geffen School of Medicine, University of California at Los Angeles, 100 Stein Plaza, Los Angeles, CA, 90095, USA.
E-mail address: radu@jsei.ucla.edu (R.A. Radu).

https://doi.org/10.1016/j.redox.2020.101787
Received 29 August 2020; Received in revised form 30 October 2020; Accepted 3 November 2020
Available online 10 November 2020

oxidized-bisretinoids were reported to induce complement activation in cultured RPE cells [15,16]. Our previous work showed that normal human RPE cells exposed to *Abca4*$^{-/-}$ photoreceptor cells OS adaptively increased expression of both anti-oxidative-stress and complement regulatory proteins genes. In contrast, the RPE cells carrying a disease-causing mutation in complement factor H (CFH) showed their inability to mount adaptive regulatory responses manifesting in an excessive membrane attack complex (MAC or C5b-9) deposition on the RPE cells following incubation with OS-containing bisretinoids [17]. These results strongly suggest that accumulation of bisretinoids causes both oxidative stress and complement dysregulation in the RPE cells. Thus, like age-related macular degeneration (AMD), Stargardt macular degeneration may be caused by persistent inflammation of the RPE.

RPE cells are known to express the complement proteins necessary for maintaining the physiological immune response throughout our lifetime [18]. The complement system is the first line of defense against pathogens invading our body [19]. Mutations in genes encoding complement-related proteins were reported to be strongly associated with AMD [20–23]. In particular, a single nucleotide polymorphism at codon 402 of CFH seemed to be responsible for ~50% of late AMD cases [24]. CFH is a major negative regulatory protein playing a key role in modulating the complement cascade via the alternative pathway. Given its structure, CFH has the ability to function both in a fluid-phase and at the cellular membrane to regulate both spontaneous C3 activation and amplification of C3 cleavage [25]. Thus, CFH-dependent activity has significant impact on the extent of cellular deposition for both MAC formation, the final product of C3 activation cascade, and C3 cleavage products [26]. Furthermore, proteomic and immunohistological analysis of postmortem tissue from patients with AMD evidenced chronic inflammatory markers and complement-related proteins [27–31]. In the STGD mouse model (*Abca4*$^{-/-}$), we observed elevated C3 cleavage products deposited on the basolateral membrane of the RPE cells [8]. These C3 fragments appeared to be internalized by the RPE and colocalized with the 488 nm autofluorescent material visualized by confocal microscopy. Despite this amplified C3 activity, STGD mice displayed a reduced level of expression for the complement regulatory proteins, including CFH, suggesting a deficiency in the complement system [8]. In a subsequent study, we used a gene-based approach to deliver a major murine complement regulator into the subretinal space and observed significant rescue of the *Abca4*$^{-/-}$ phenotype, including RPE bisretinoid reduction and photoreceptor degeneration [32]. These findings suggest that local RPE complement dysregulation is a causal factor in the pathogenesis of STGD, similar to AMD. In this report, we performed immunohistochemical analysis to investigate and to quantify key complement-related proteins (MAC, C3, and CFH) in postmortem fixed tissue from three donor eyes of patients clinically diagnosed with Stargardt disease.

2. Material and methods

2.1. Human donor tissue

Human donor eyes were obtained from the Cole Eye Institute Eye Tissue Repository obtained through the Foundation Fighting Blindness (FFB) Rare Eye Donor Eye program (Columbia, MD), Cleveland Eye Bank (Cleveland, OH), and University of Utah Salt Lake City (generous gift of Dr. Gregory Hageman). Immunohistochemical and histological analysis were performed with the approval of the Cleveland Clinic Institutional Review Board (IRB #14-057). The research adhered to the tenets of the Declaration of Helsinki. Donor eyes were clinically diagnosed as Stargardt disease (STGD) without known genotype. A limited amount of DNA was extracted from fixed tissue and subjected to genotype analysis for *ABCA4*, responsible for recessive Stargardt disease, and *CFH*, a gene associated with AMD. Donor eye phenotype, age, source, genotype (*ABCA4* and *CFH*) and label identification used in the current study is provided in Table 1. DNA isolated from both donor eyes STGD #2 and STGD #3 were sent to Blueprint Genetics Laboratories (San Francisco, CA) for analysis in a Macular Dystrophy Panel Plus (a 28 gene panel that includes assessment of non-coding variant). Samples were also screened for single nucleotide polymorphisms (SNPs) correlated with AMD (Table 2) as previously described [28].

2.2. Immunohistochemistry

Eyes were enucleated within 6–48 h postmortem interval (Table 1), fixed in 4% paraformaldehyde and 0.5% glutaraldehyde in Dulbecco's phosphate buffered saline (PBS), and shipped overnight. On receiving, globes were cut through ora serrata, washed with PBS, and stored in 2%

Table 1
Human donor eye additional information.

Phenotype	Age (yr)[a]	Source	*ABCA4*	*CFH* 402	*CFH* 62	D-to-P[b] (hrs)	Donor Eye ID current study
	Gender		Genotype	Genotype	Genotype		
Normal	65-U[c]	FFB # 696	–	YH	IV	10	CTRL
Normal	66-F	Cleveland Eye Bank	–	HH	IV	8	CTRL #1
Normal	84-F	FFB #1022	–	YH	IV	10	CTRL #2
Normal	52	Univ. Utah	–	N.D.[d]	N.D.[d]	N.D.[d]	CTRL #3
Normal	65- A[e]	FFB #654	–	N.D.[d]	N.D.[d]	24	CTRL #4
Normal	68-A[e]	FFB #635	–	N.D.[d]	N.D.[d]	34	CTRL #5
Stargardt	66-F	FFB #863	G1961E and IVS46 + 2 (C > G)[f]	HH	VV	18	STGD #1
Stargardt	69-M	FFB #1012	–	HH	VV	33	STGD #2
Stargardt	72-M	FFB #878	Novel mutation[g] heterozygous mutation (c.629C > G, p. Pro210Arg) in the *PRPH2*	HH	VV	48	STGD #3

[a] Age: age at death (years) and gender: M = male, F = female.
[b] Interval from death (D) to preservation (P) in hours (hrs).
[c] U: Unknown.
[d] N.D.: Not determined.
[e] A: Anonymous.
[f] As previously reported in Bonilha et al. [34].
[g] Determined by a Macular Dystrophy Panel from Blueprint Genetics Lab. *ABCA4* non-coding variants covered in this analysis included: c.6730-19G > A; c.6148-471C > T; c.6148-471C > T; c.5196 + 1137G > A; c.5196 + 1137G > T; c.5196 + 1056A > G; c.4539 + 2065C > G; c.4539 + 2064C > T; c.4539 + 2028C > T; c.4539 + 2001G > A; c.4539 + 1928C > T; c.4539 + 1729G > T; c.4539 + 1106C > T; c.4539 + 1100A > G; c.4253 + 43G > A; c.3191–11T > A; c.3051-16T > A; c.3050 + 370C > T; c.2919-383C > T; c.2160 + 584A > G; c.1938-619A > G; c.1937 + 435C > G; c.1937 + 13T > G; c.859-506G > C; c.859–540C > G; c.769–784C > T; c.768 + 3223C > T; c.570 + 1798A > G; c.302 + 68C > T; c.161–23T > G; c.67-16T > A.

Table 2
Human donor genotyping for additional SNPs correlated with AMD[a].

Donor[a]	ARMS2	C3	HTRA	SOD2	MBP	C80rf42
Eye ID	A69S	R80G	Promoter			
CTRL	GT	CC	AG	AA	AC	AC
CTRL #1	GT	GG	GG	GG	CC	CC
CTRL #2	GG	CC	GG	AG	AC	CC
CTRL #3	N.D.[b]	N.D.[b]	N.D.[b]	N.D.[b]	N.D.[b]	N.D.[b]
CTRL #4	N.D.[b]	N.D.[b]	N.D.[b]	N.D.[b]	N.D.[b]	N.D.[b]
CTRL #5	N.D.[b]	N.D.[b]	N.D.[b]	N.D.[b]	N.D.[b]	N.D.[b]
STGD #1	GG	CC	GG	AG	AA	CC
STGD #2	CC	CG	GG	AG	AC	CC
STGD #3	GG	CC	GG	AG	CC	CC

Red font signifies risk alleles.

[a] Donor samples were genotyped for single nucleotide polymorphisms (SNPs) correlated with AMD (*ARMS2* - age-related maculopathy susceptibility 2, *HTRA1* - high temperature requirement factor A1, and *C3* – complement component 3) and for SNPs previously shown to be associated with GA (near *SOD2* - Superoxide dismutase 2; near *MBP* - myelin basic protein; near *TDRP* - testis development related protein).

[b] N.D.: Not determined.

paraformaldehyde until further use. Tissue fragments of retina-RPE-Choroid (~5–10 mm^2 pieces) from the perimacular (PM) and peripheral (P) regions were transferred then incubated overnight in PBS, washed three times with PBS, infiltrated with 10–30% sucrose in PBS, embedded in Optimal Cutting Temperature medium (Fisher Health care, Huston, TX) and then cut into 12-μm sections. Some heavily pigmented RPE sections were bleached for 3–5 min using the Melanin Bleach Kit (Polysciences). After washing in 3x with phosphate buffer, frozen sections were quenched with 50 mM NH_4Cl, blocked with 5% goat or donkey serum with 1% BSA in PBS. The sections were then exposed to the primary antibody overnight at 4 °C, washed, and incubated with the secondary antibody-conjugated Alexa Fluor dye for 1 h at room temperature. All sections were stained with DAPI nuclear marker (Invitrogen) and mounted with 5% n-propyl gallate in 100% glycerol. RPE pieces were fixed as described above with addition of a detergent permeabilization step (1% Triton X-100 for 1 h at room temperature), blocked overnight with 1% BSA/5% goat serum/0.5% Triton X-100 in PBS buffer and incubated with 4-HNE antibody for three days at 4 °C. A list of both primary and secondary antibodies, experimental dilution, and their sources are provided in Table 3.

2.3. Confocal microscopy analysis

Images were captured using an Olympus FV 1000 confocal microscope (60x objective). RPE autofluorescence was detected by excitation with a 488-nm (argon) laser with a 520-nm emission filter. Immunostaining signals were captured at excitation wavelengths of 559- or 635-nm and emission wavelengths of 618- or 668-nm respectively and the images were analyzed using the FV1000 software. Pixel intensity values in normal donor (control) and STGD donor sections were analyzed to determine the C5b-9 (MAC), C3b/iC3b fragments, and CFH relative levels. The average was obtained by quantifying intensities in 10 regions from each section in each donor in the peripheral region; a total of 3–14 sections were analyzed for the control and STGD eye donor. Individual data point of control and STGD groups was normalized to the average of control intensity value for each experiment. The results are presented as mean ± S.D. Statistical analysis was performed using the Student's *t*-test.

2.4. Electron microscopy analysis

Fragments of retina-RPE-choroid were fixed in 2.5% glutaraldehyde in 0.1 M cacodylate buffer. After dehydration in ethanol, the tissue fragments were embedded in Epon as previously reported [33]. Ultrathin sections were cut on a Leica Ultracut ultramicrotome, collected on 200-mesh copper grids, and stained with uranium and lead salts. The images for Stargardt donor eye #1 (STGD #1) and control (CTRL #1) were captured at 15,000x using a JEM 1200-EX electron microscope (JEOL, Peabody, MA) with wide angle (top mount) and the BioScan 600 W 1x1K digital camera (Gatan) and Digital Micrograph acquisition software (Gatan). The images for Stargardt donors' eyes #2 and #3 (STGD #2 and STGD #3) and corresponding control eyes (CTRL #2i and CTRL #2ii) were collected using a JEM-1400 electron microscope (JEOL Peabody, MA) with ORIUS SC1000b Camera and Gatan Microscopy Suite Software (Gatan, Inc., Pleasanton, CA).

3. Results

3.1. Ultrastructural features of the RPE cells in the peripheral region

All three globes displayed different levels of central atrophy of the retina by fundus macroscopy: STGD #1 showed a classic STGD phenotype with severe RPE loss and hyperpigmentation in the perimacular region [34]; STGD #2 exhibited a small parafoveal atrophic area while STGD #3 displayed a large region of macular atrophy [35]. Genetic information could not be collected for STGD #2 due to the poor DNA quality while STGD #3 was found to carry a heterozygous mutation (c.629C > G, p.Pro210Arg) in the *PRPH2* gene. Hence, although all three donors were clinically diagnosed with STGD, only one could be genetically classified as STGD. We then performed electron microscopic (EM) analysis of the peripheral area to document the RPE morphological features of our STGD donor eyes before investigating complement immunoreactivity. EM analysis evidenced an elevated number of electron-dense, irregular shaped lipofuscin granules (yellow arrowhead) distributed throughout the RPE in the STGD #1 to #3 eyes (Fig. 1, bottom panels) vs controls (Fig. 1, top panels). STGD #1 also displayed frequent clusters of lipofuscin granules in its cytoplasm when compared to STGD #2 and #3. Melanolipofuscin (cyan arrowhead) structures appeared to be more abundant in STGD #1 to #3 donor eyes vs controls. These findings are consistent with previously reported ultrastructural analysis of the STGD #1 donor eye [34].

Table 3
List of antibodies used for immunohistology in this study.

Primary Antibody	Company	Catalog #	Dilution	SecondaryAntibody	Company	Catalog #	Dilution
C5b-9 (MAC) Monoclonal mouse anti-human C5b-9 (clone aE11)	DAKO	M-0777	1:50	Goat anti-mouse IgG conjugated to Alexa Fluor 647	Invitrogen	A-21236	1:500
iC3b Monoclonal antibody to human iC3b	Quidel	A-209	1:100	Goat anti-mouse IgG conjugated to Alexa Fluor 647	Invitrogen	A-21236	1:500
CFH Polyclonal antiserum to human **CFH**	Quidel	A-312	1:250	Donkey anti-goat IgG conjugated to Alexa Fluor 594	Invitrogen	A-11058	1:500
4-HNE Monoclonal antibody (12F7)	ThermoFisher	MA5-27570	1:50	Goat anti-mouse IgG conjugated to Alexa-647	Invitrogen	A-21236	1:500

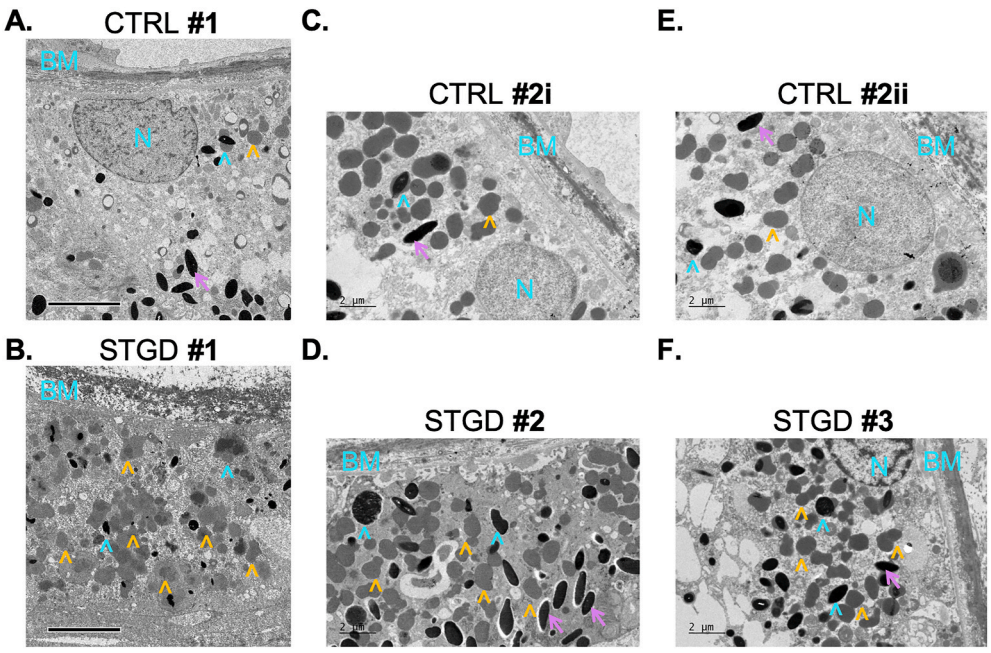

Fig. 1. Electron microscopic analysis of the peripheral region of human donor eyes. Representative electron microscopic images of RPE cells in the peripheral region of control (CTRL, top panels, **A, C, E**) and Stargardt (STGD, bottom panels, **B, D, F**) donor eyes. Lipofuscin (yellow arrowheads) and melanolipofuscin (cyan arrowheads) granules are more abundantly distributed in the RPE cells of Stargardt donor eyes (B, D, F) vs control eyes. Purple arrows indicate melanosomes; Nucleus (N); Bruch's membrane (BM); Scale bar = 2 μm. (For interpretation of the references to colour in this figure legend, the reader is referred to the Web version of this article.)

3.2. MAC-mediated morphological changes are evidenced in STGD perimacular region

The initial complement study involved both perimacular and peripheral regions of the STGD #1 donor eye previously genotyped and reported as a heterozygous compound with two mutations in the *ABCA4* gene (p.Gly1961Glu and IVS46 + 2 C > G) [34]. Control tissue was obtained from a postmortem eye of a donor without a history of retinal disease or known ABCA4 variants. Fundus photographic analysis of the STGD eye showed visible RPE atrophic regions within the macula which were not suitable to interrogate complement reactivity [34]. Our early investigation of MAC deposition was directed to the perimacular region with a reduced degree of RPE cell loss (Fig. 2). While the control donor eye (CTRL) displayed the RPE cells in a monolayer (Fig. 2, top panels), we observed significant morphological changes of both RPE and Bruch's membrane (BM) in the perimacular region of the STGD #1 (Fig. 2, bottom panels). Particularly, the pentalaminar layers of BM appeared to be disorganized, with intermittent breakage (white arrowhead), and an overall increased thickness due to invasion of new choroid blood vessels (yellow asterisks). Distortion of the adjacent RPE monolayer with hypertrophic cells was also observed in the STGD #1 donor eye. Immunostaining with an antibody against complement complex C5b-9 (or MAC) showed substantial C5b-9 deposition predominantly on the distorted layers of the BM and on the basal membrane of the RPE cells of STGD #1 (Fig. 2, yellow arrows). In contrast, the CTRL donor eye showed C5b-9 immunoreactivity on the choriocapillaris (CC) endothelium beneath an intact BM (yellow arrowhead) and very little to none on the RPE (Fig. 2, top panels). Difference in time between death-to-preservation (D-to-P) of the control vs STGD donor eye, at 10-hr and 18-hr respectively, prompted us to evaluate the MAC staining using retina sections from additional non-Stargardt control donor eyes with a D-to-P of 24-hr and 34-hr (Supplementary Fig. S1). We found that

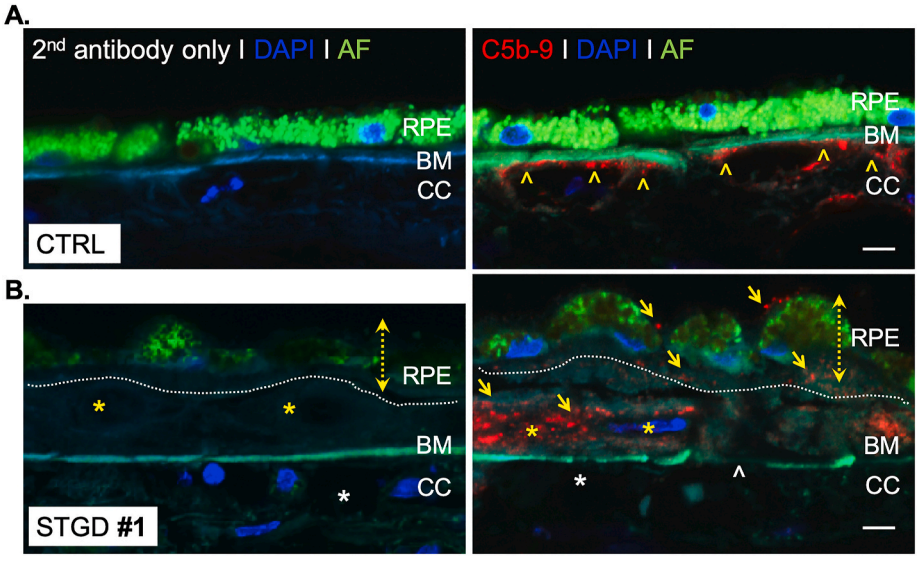

Fig. 2. Membrane attack complex localizes on the disrupted RPE cells in the perimacular region of the Stargardt donor eye. Representative merged confocal images of frozen sections of human retina from the perimacular region of the donor eyes: control (**A**) (CTRL, top panels) and Stargardt disease (**B**) (STGD #1, bottom panels) stained with an antibody against C5b-9 (MAC, red) and endogenous autofluorescence (AF) acquired at 488 nm. Nuclei are stained with DAPI (blue). Images on the left correspond to CTRL and STGD #1 sections respectively without the primary antibody (2nd antibody only). Note: in the control section MAC predominantly deposits on the endothelia (yellow arrowheads) lining the choriocapillaris (CC) unlike the STGD section that showed a heterogeneous distribution (yellow arrows) on the distorted RPE cells and thicken Bruch's membrane (BM) invaded by new blood vessels indicated by a yellow asterisk (*). Dotted white line delineates basal membrane of the RPE cells. White arrowhead denotes a break in the Bruch's membrane; white asterisk (*) points to a choriocapillaris atrophy. Scale bar = 10 μm. (For interpretation of the references to colour in this figure legend, the reader is referred to the Web version of this article.)

longer time to preservation in fixative after death did not significantly change the immunogenicity of MAC for the RPE cells (Supplementary Fig. S1).

3.3. MAC distribution in the peripheral region

Due to significant RPE cellular disruption and areas of neovascularization in the perimacular region of the STGD eyes, immunochemistry quantitation of C5b-9 deposition was not possible. We then assessed C5b-9 immunolabeling in the peripheral region containing a monolayer of RPE cells, confirmed in our preliminary ultrastructural evaluation by EM analysis (Fig. 1). Sections from STGD (#1, #2, #3) and the corresponding control (CTRL #1, #2, #3) eyes were analyzed independently. C5b-9 immunolabeling was evident in the RPE of all STGD sections and mostly absent from the RPE of the control sections (Fig. 3A, 3C, 3E). Fluorescence intensity quantification of C5b-9 deposition on the RPE cells was significantly increased in STGD eyes vs controls (Fig. 3B, 3D, 3F). Furthermore, average data from all three eyes of each group showed about 1.6-fold higher C5b-9/MAC levels in STGD compared to the control eyes ($p < 0.02$, n = 3 eyes, 25 sections for each control and STGD group, Supplementary Fig. S2A).

3.4. C3/C3b/iC3b distribution in the peripheral region

Increased MAC deposition in the STGD donor eyes reflects a chronic over-amplified complement cascade initiated by C3 convertase (C3b). To investigate the C3b inactivation, we used immunohistochemistry to quantify the C3 break-down fragment levels in the RPE of the peripheral region (Fig. 4). Immunoreactivity of C3b/iC3b in STGD #1 and #3 displayed patchy accumulation within the cell cytoplasm (Fig. 4A and 4E). In the case of STGD #2 eye, we observed a more homogeneous distribution of C3b/iC3b staining similar to the CTRL #2 sections (Fig. 4C). For STGD #1 eye, we measured an approximate 1.5-fold increase vs control C3b/iC3b levels (Fig. 4B). Although a statistical significance was evidenced in STGD #1 (Fig. 4B, $p = 0.037$, n = 8 sections), the C3b/iC3b profile was dissimilar in STGD #2 (Fig. 4D, $p = 0.129$, n = 6 sections) and STGD #3 (Fig. 4F, $p = 0.08$, n = 3 sections) suggesting either a different C3 reactivity on the RPE cell membrane or a change in RPE intracellular processing rate of the internalized C3 fragments. Consequently, the average data from all three STGD eyes showed a trend toward increased C3 breakdown products within the RPE cells without a statistically significant relevance ($p = 0.16$, n = 3 eyes, 17 sections for each control and STGD group, Supplementary Fig. S2B).

3.5. CFH distribution in the peripheral region

As the C3 inactivation process requires CFH as a cofactor, we assessed CFH immunoreactivity in the peripheral region of STGD and control donor eyes. Genetic analysis showed that all three STGD donor eyes carry the CFH risk-genotype HH402 (Table 1). CFH distribution and quantitative levels in the RPE cells was significantly diminished in all STGD eyes vs control eyes ($p < 0.003$, n = 3 eyes, 23 sections, Supplementary Fig. S2C). However, quantification of individual eye CFH immunostaining signals indicated that only two of the donor eyes, STGD #1 ($p = 0.011$, n = 12 sections) and STGD #2 ($p = 0.037$, n = 8 sections) reached statistical significance (Fig. 5). Analysis for single nucleotide

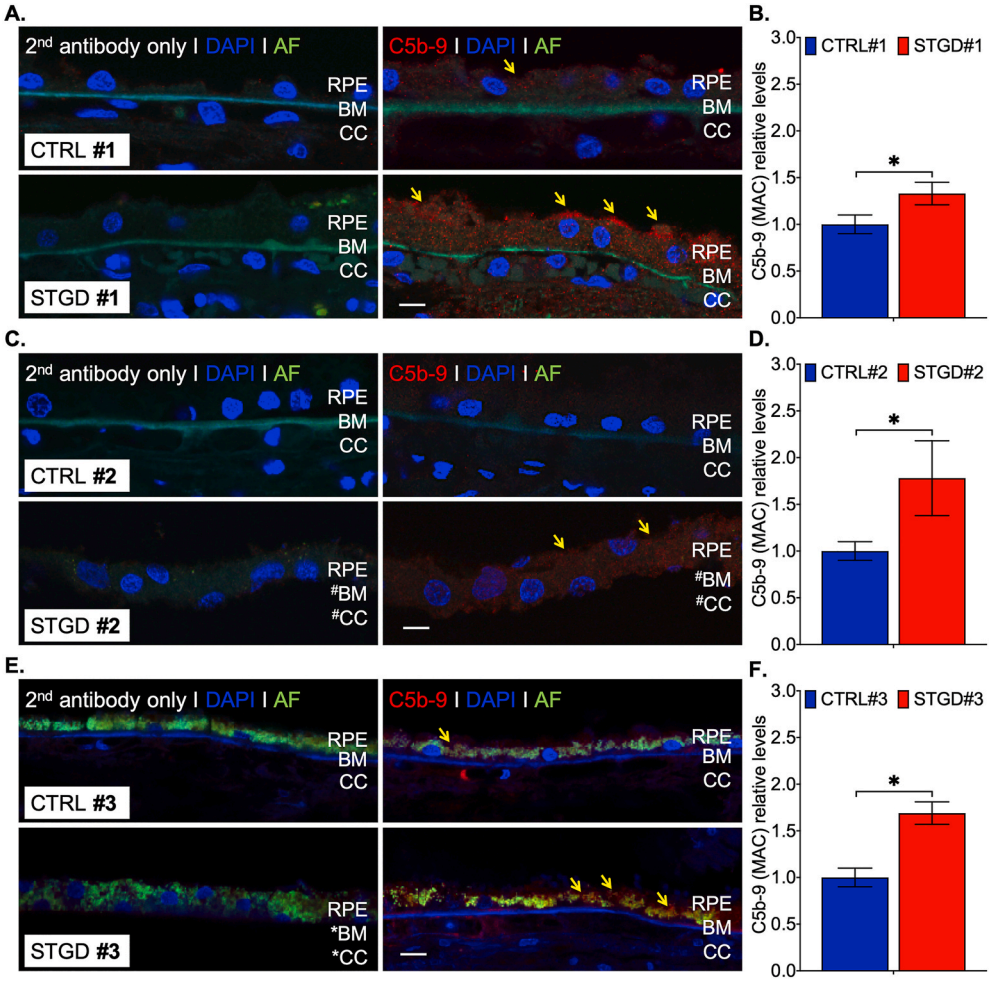

Fig. 3. Accelerated deposition of membrane attack complex on the RPE cells of Stargardt donor eyes. Representative merged confocal images of peripheral retina sections of Control (CTRL) and Stargardt (STGD) donor eyes (**A, C, E**) immunostained with an antibody against C5b-9 (right) and without a primary antibody (left, secondary (2nd) antibody only). Corresponding histograms for C5b-9 (MAC, red) levels based on the pixel intensity quantification are shown in **B, D, F**. Note: all Stargardt donor eyes present significantly higher MAC immunoreactivity compared to the control eyes. Autofluorescence (AF) was acquired at 488 nm. Sections in panel A and C were bleached to reduce the AF signal. Nuclei are stained with DAPI (blue). Yellow arrows indicate areas of C5b-9 (MAC) staining. Scale bar = 20 μm; (#) indicate missing tissue. Data presented as mean ± S.D.; n = 25 sections for each control and STGD group; *$p <$ 0.005. (For interpretation of the references to colour in this figure legend, the reader is referred to the Web version of this article.)

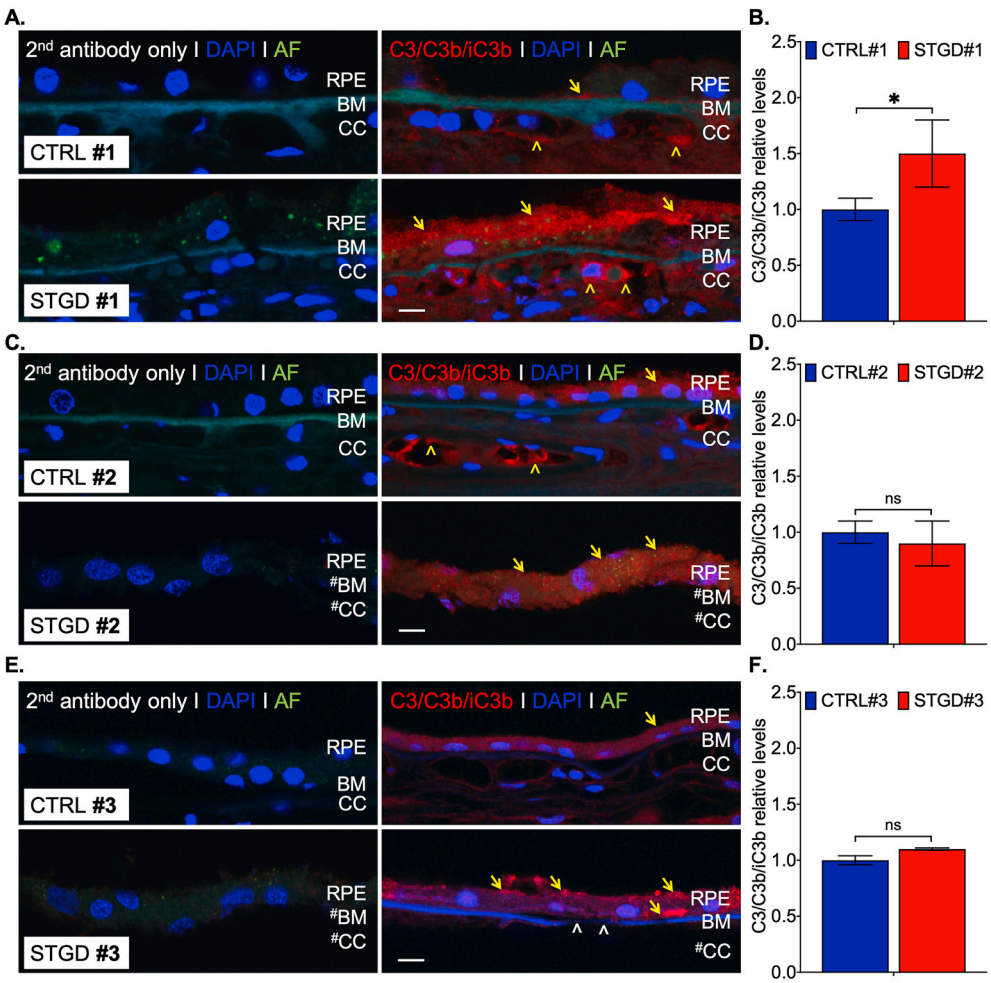

Fig. 4. C3/C3b/iC3b immunohistochemistry in the peripheral region of the human eye donors. Representative merged confocal images of peripheral retina sections of Control (CTRL) and Stargardt (STGD) donor eyes (**A, C, E**) immunostained with an antibody against C3/C3b/iC3b (right) and without a primary antibody (left, secondary (2nd) antibody only). Corresponding histograms for C3 (red) levels based on the pixel intensity quantification are shown in **B, D, F**. Note: only the STGD #1 donor eye showed statistical significance in C3 levels. Autofluorescence (AF) was acquired at 488 nm. All sections were bleached to reduce the AF signal. Nuclei are stained with DAPI (blue). Yellow arrows and arrowheads indicate areas of C3/C3b/iC3b staining in the RPE and choroid capillaries (CC) respectively; white arrowheads indicate breaks in Bruch's membrane (BM). Scale bar = 20 μm; (#) indicate missing tissue. Data presented as mean ± S.D.; n = 4–8 sections for each control and STGD group; *p < 0.05; n.s. = not statistically significant. (For interpretation of the references to colour in this figure legend, the reader is referred to the Web version of this article.)

polymorphism in genes associated with AMD evidenced other risk alleles for both control and STGD eyes (Table 2). Taken together, these data further indicate an RPE-specific complement reactivity may involve additional intracellular players.

3.6. 4-Hydroxynonenal (4-HNE) distribution in the peripheral region

In the STGD mouse model, the bisretinoid-lipofuscin buildup was also associated with an increase in oxidative stress markers such as malondialdehyde (MDA) and 4-HNE, both natural byproducts of lipid peroxidation. We prepared RPE flatmounts from the peripheral region of the donor eyes and stained for 4-HNE. The intensity of the 4-HNE staining was variable in the RPE flatmounts of STGD eyes suggesting more factors may be implicated in sustaining RPE cell homeostasis as a function of each donor genotype. Despite this degree of heterogeneity and visible RPE cells loss, all STGD donor eyes displayed stronger immunoreactivity for 4-HNE staining when compared to the control eye (Fig. 6).

4. Discussion

This manuscript presents a biochemical characterization of key molecular markers of the complement system in the RPE cells from three postmortem donor eyes with Stargardt disease. To our knowledge, this is the first report to investigate and to quantify the complement-related proteins (C5b-9, C3, and CFH) in postmortem fixed tissue from three donor eyes of patients clinically diagnosed with Stargardt disease. Previously, there were just two reports describing the histopathology in neural retinas from STGD donor eyes [34,36,37]. The first histopathologic study was carried out in a donor eye for which there was no genetic information available. The retina of this donor eye exhibited elevated levels of lipofuscin granules in the peripheral RPE and surviving photoreceptor cells. However, in the macular region of this donor eye, there was a significant loss of RPE, Muller cell hypertrophy, and rod and cone photoreceptors with abnormal structure [36]. The second histopathological study involved a donor eye that was genetically screened and found to be compound heterozygous for *ABCA4* and was included in the current report (STGD #1). All published morphological findings are consistent to the ones we described in our STGD donor eyes.

Studied STGD donors received a diagnosis of STGD based on the age of each subject at the initial ocular evaluation validating a typical macular pathology involving atrophy of perifoveal and foveal regions [38,39]. Clinical presentation of STGD ranges from early-onset loss of the foveal region expanding to the peripheral retina over time to late-onset mild cases of central retinal atrophy. These diverse clinical appearances are likely due to extensive *ABCA4* disease-associated genetic variations [40,41]. Presently, more than 1000 disease-causing variants have been identified in the coding sequences and splice sites of the *ABCA4* gene [42]. *ABCA4* is also a rare susceptibility locus for a sub-group of patients with AMD with geographic atrophy (GA) suggesting common etiology with STGD [43]. Dysfunctional ABCA4 causes abnormal accumulation of toxic autofluorescent bisretinoid-lipofuscin material in the cells of the RPE in an age-dependent fashion [12,44,45]. This RPE accumulation is often visualized as flecks of increased fundus autofluorescence when employing an excitation wavelength for detection of bisretinoids [46]. Fundus autofluorescence analysis can also

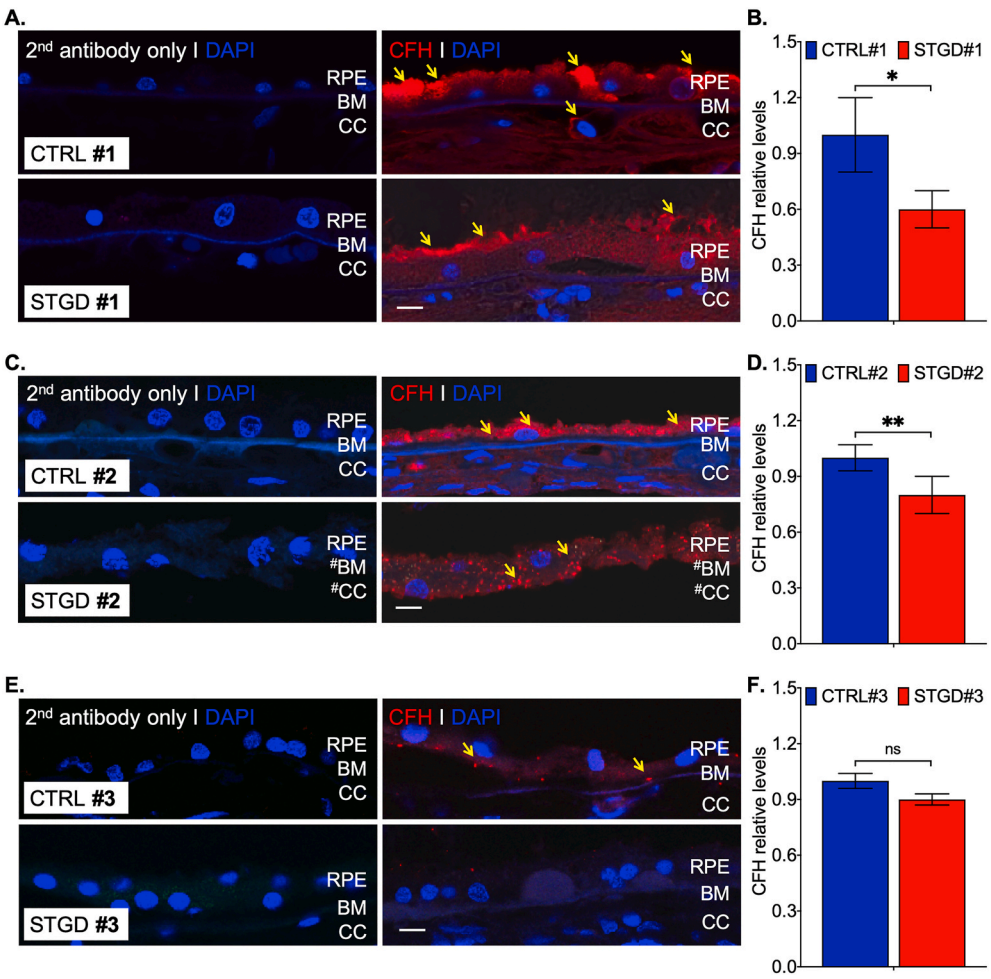

Fig. 5. Complement factor H levels are reduced in the RPE cells of Stargardt donor eyes. Representative merged confocal images of peripheral retina sections of Control (CTRL) and Stargardt (STGD) donor eyes (**A, C, E**) immunostained with an antibody against CFH (right) and without a primary antibody (left, secondary (2nd) antibody only). Corresponding histograms for CFH (red) levels based on the pixel intensity quantification are shown in **B, D, F**. Note: all Stargardt donor eyes displayed reduced levels of CFH in the RPE cells. Autofluorescence (AF) was acquired at 488 nm. All sections were bleached to reduce the AF signal. Nuclei are stained with DAPI (blue). Yellow arrows indicate areas of CFH staining in the RPE and choroid capillaries (CC). Scale bar = 20 μm; (#) indicate missing tissue. Data presented as mean ± S. D.; n = 3–14 sections for each control and STGD group; *p < 0.01; **p < 0.05; n.s. = not statistically significant. (For interpretation of the references to colour in this figure legend, the reader is referred to the Web version of this article.)

reveal regions of decreased or absent fluorescence due to RPE atrophy [47,48]. Recently, extensive histopathology analysis of postmortem eyes of AMD donors with GA revealed enhanced autofluorescence material within the RPE cells surrounding the GA lesions, further supporting similar pathogenic mechanism as STGD [28].

In our study, genetic testing confirmed a STGD diagnosis only in the STGD #1 donor eye, which harbored two heterozygous *ABCA4* mutations (p.Gly1961Glu and IVS46 + 2 C > G) as previously reported [34]. Histological analysis showed a severely degenerated fovea with little evidence of any retinal layering or remaining RPE. The perifoveal region contained a few cones and residual rods, and decreased autofluorescence of the RPE, consistent with substantial cellular loss. In contrast, the periphery displayed stubby cones, decreased rhodopsin-labeled cells and increased autofluorescent granules in the RPE [34]. Extracted DNA from the STGD #2 eye donor was not qualitatively sufficient to determine the ABCA4 genotype while the STGD #3 eye donor was found to harbor a *PRPH2* mutation. Mutations in the *PRPH2* gene cause multifocal pattern retinal degeneration and central areolar choroidal dystrophy, simulating a fundus flavimaculatus retinopathy [49–51]. The *PRPH2* gene encodes a protein called peripherin 2 expressed in the outer segments of both rod and cone photoreceptor cells. Peripherin 2 protein is essential for formation and structural stability of the highly organized stackable disk membranes of these light-sensitive cells [52]. Notably, a sub-group of patients carrying PRPH2 variants manifest with an RPE pattern dystrophy characterized by abnormal autofluorescent material buildup similar to a classic phenotype of recessive STGD [53]. Other causal genes, including known retinal disease genes (CRX, CRB1, RDH11, etc), were also identified using the whole-exome sequencing approach for patients with STGD-like phenotype [54–56]. Additional genetic studies indicated that a small fraction of clinically diagnosed STGD patients still cannot be associated with any ABCA4 disease-causing variants [57].

We further validated the initial clinical diagnosis of STGD for these donor eyes by employing an ultrastructural analysis in the peripheral region that retained a monolayer of RPE cells. Here, we showed that electron-dense lipofuscin and melanolipofuscin granules, both key pathological hallmarks for STGD, were much more abundant in the STGD donor eyes versus control eyes. Additional morphological features of the same STGD donor eyes were described in a recent study by Edwards et al. [35]. Analyzing the flatmounts of both retinas and choroids from these STGD donor eyes, they evidenced severe attenuation of the choriocapillaris in areas with RPE loss. Furthermore, they found that the area of RPE atrophy was accompanied by an extension of Müller cell processes into the subretinal compartment unlike the area with an intact monolayer which displayed choriocapillaris with normal density and lumenal diameter [35]. Previously, Taubitz et al. reported severely degenerated photoreceptors resulting in geographic atrophy in the macula of the STGD #3 retina, a typical clinical appearance for Stargardt patients [37]. Importantly, the areas containing RPE cells showed significant lipofuscin and melanolipofuscin deposition [37]. Consequently, we focused our studies on the peripheral region which retained a relatively normal morphological appearance of the RPE cells. In this peripheral region, STGD donor eyes displayed notable increase oxidative stress markers likely due to the buildup of bisretinoid-lipofuscin granules in the RPE cells. The observed heterogeneity of the 4-HNE immunostaining strongly argues for a complex pathophysiology of STGD as a

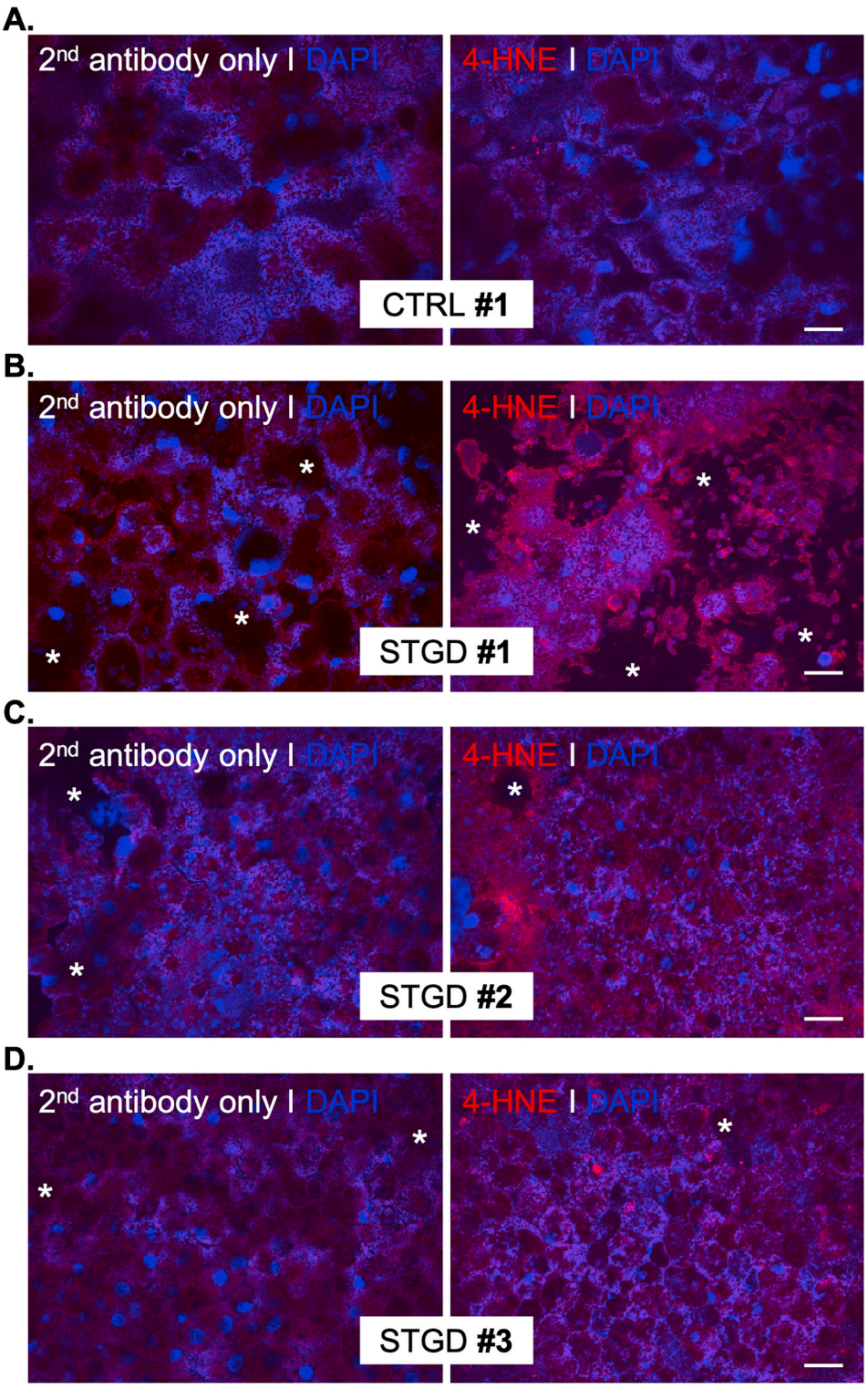

Fig. 6. Increased oxidative stress is evidenced by 4-hydroxynonenal immunostaining in the RPE cells of Stargardt donor eyes. Representative merged confocal merged images of flatmount punches of the Control (**A**) and Stargardt donor eyes (**B-D**) from the peripheral region immunostained with an antibody against 4-HNE (right) and without a primary antibody (left, secondary (2nd) antibody only). Note: strong immunoreactivity for 4-HNE is evidenced in all Stargardt donor eyes compared to the control donor eye. Nuclei are stained with DAPI (blue). White asterisk (*) indicates missing RPE cells. Scale bar = 20 μm; n = 3 punches for each control and STGD donor eyes. (For interpretation of the references to colour in this figure legend, the reader is referred to the Web version of this article.)

function of each patient's genetic background.

The RPE is an important regulator of the ocular immune response. Multiple components of the complement pathway are expressed in RPE cells, including secreted CFH [18,58]. The CFH gene is a known susceptibility locus for AMD. In particular, the Y402H substitution is represented in a significant fraction of AMD cases [21,59]. Genetic analysis showed that STGD donor eyes involved in this study carry the CFH risk-allele with reduced secreted protein levels. This genetic background raised the question whether these STGD eyes may have been exposed to chronic local inflammatory reactivity with sub-lytic MAC deposition on the RPE cells. Complement cascade is activated via multiple pathways and culminates with the assembly of MAC, a complex of C5–C9 fragments, on the cellular membrane [60]. A functional RPE can mitigate an abnormal complement attack due to MAC deposition on the cell surface by internalizing and processing MAC via an endocytic pathway [61]. Here, STGD eye donors showed significantly enhanced MAC accumulation on the RPE cells and an approximate 1.6-fold higher level of internalized MAC by the RPE cells. These data suggest an overly

amplified C3 complement cascade initiated on the RPE cell membrane due to accumulation of bisretinoid-lipofuscin.

Increase in complement-related protein transcripts were previously reported in an eye donor diagnosed with autosomal recessive retinitis pigmentosa, known as heterozygous compound due to two ABCA4 disease-causing mutations on different allele [62]. Histological characterization of this eye donor revealed a complete loss of photoreceptors and increased autofluorescence in the residual RPE cells [62]. Taken together, these findings suggest a strong immune reactivity of the RPE cells in response to the endogenously built-up bisretinoid-lipofuscin. Activation of C3 complement by bisretinoids was previously showed in cultured RPE cells [15,16]. Increased C3 complement activity was also evidenced in the RPE cells of the *Abca4*$^{-/-}$ mouse, a model of STGD [8]. Interestingly, substantial C3 fragments were internalized by the RPE and overlapped with the autofluorescent material in the STGD mouse eyes [8]. Similarly, the STGD #1 donor eye displayed considerably elevated C3b/iC3b levels compared to the corresponding control, a profile that was not observed in the other two STGD donor eyes. This discrepancy may be caused by differences in the genetic background for *ABCA4*, *CFH*, and other AMD-associated genes which likely dictate the RPE reactivity for both pathways to activate and regulate the complement system.

Augmented inflammatory markers were also reported in the eyes of *Abca4*$^{-/-}$ mice [8]. Degeneration of photoreceptors in these animals has been attributed to a decline in RPE function due to chronic bisretinoid-mediated complement dysregulation [32]. Moreover, *Abca4*$^{-/-}$ mice exhibited age-dependent increased oxidative stress, evidenced by the accumulation of MDA and 4-HNE in the RPE cells [8]. These lipid peroxidation byproducts could poison the RPE cells via an aldehyde-based cytotoxicity mechanism. It has been shown that CFH binds MDA, reducing its potential for further oxidative damage [63]. Our previous studies indicated that cultured RPE cells can secrete similar CFH levels irrespective of their CFH Y402H genotype [17]. However, under stressful conditions such as a single ingestion of OS containing bisretinoids, the RPE cells caring the AMD-risk CFH variant were unable to block MAC formation due to reduced levels of endogenously released CFH [17]. Lower levels of CFH were also observed in our analyzed STGD donor eyes. This finding reflects an ongoing inability of the RPE cells to locally regulate the complement system due to a notable bisretinoid-lipofuscin accumulation in the STGD donor eyes.

Given the heterogeneity in the STGD clinical presentations and patient genetic variations, the necessity of developing STGD patient-derived RPE cells is crucial to expand the investigation of the complement dysregulation evidenced in the eyes from both STGD donor eyes and STGD mouse model. Steps toward establishing intrinsically pluripotent stem cells (iPSC) from STGD patients have already been initiated in many laboratories, including ours. Preliminary analysis of an iPSC-derived RPE cell-based STGD model demonstrated key phenotypic features of STGD disease, such as increased autofluorescence, cellular dysmorphism and atrophy. Ongoing studies are directed to interrogate the bisretinoid-mediated complement activity and determine the local RPE-specific complement regulatory mechanism and RPE oxidoreductase activity that perturb cellular homeostasis.

Numerous studies have implicated complement-associated inflammation as a contributor to both AMD and STGD [28,64]. Altogether, our data suggest that in STGD, like AMD, the RPE cells become dysfunctional and lose their ability to suppress chronic complement attack. Ongoing bisretinoid-lipofuscin buildup within RPE cells, specific for STGD patients, leads to both oxidative stress and sublytic complement activity. With time, the RPE cellular impairment is further amplified by an insufficient complement regulatory mechanism causing lysis of the cellular membrane and subsequent RPE cell death. Loss of RPE cells, evidenced in both STGD and AMD patients, precedes functional and structural changes of photoreceptor cells that lead to blindness.

Our report points to a therapeutic strategy that targets modulation of the complement system locally in the RPE cells. Transplantation of iPSC-derived RPE cells for patients with residual functional photoreceptors is another potential beneficial therapeutic approach for STGD, AMD, and other maculopathies with early RPE cellular dysfunction. Future therapeutic advances must be directed towards promoting RPE viability and restoring physiological cellular parameters needed to preserve vision.

Acknowledgements

We acknowledge Shannan Eddington for her outstanding technical support and David Schumick for preparation of the illustrations included in the graphical abstract. This work was supported by the National Institutes of Health (EY027750 to VLB and EY025002 to RAR), National Eye Institute P30 Core Grant to the Cole Eye Institute (P30EY025585) and Stein Eye Institute Core Grant for Vision Research (EY000331), the Sarkaria philanthropic fund (RAR), Research to Prevent Blindness unrestricted grant to the Department of Ophthalmology at UCLA Stein Eye Institute, Research to Prevent Blindness challenge grant to the Cole Eye Institute and Cleveland Clinic Foundation startup funds (VLB). The authors also acknowledge the support of Foundation Fighting Blindness in setting up the Eye Tissue Repository and the Cleveland Clinic for funding its maintenance.

Appendix A. Supplementary data

Supplementary data to this article can be found online at https://doi.org/10.1016/j.redox.2020.101787.

References

[1] R. Allikmets, et al., A photoreceptor cell-specific ATP-binding transporter gene (ABCR) is mutated in recessive Stargardt macular dystrophy, Nat. Genet. 15 (3) (1997) 236–246.
[2] M. Michaelides, D.M. Hunt, A.T. Moore, The genetics of inherited macular dystrophies, J. Med. Genet. 40 (9) (2003) 641–650.
[3] P. Tanna, et al., Stargardt disease: clinical features, molecular genetics, animal models and therapeutic options, Br. J. Ophthalmol. 101 (1) (2017) 25–30.
[4] T.L. Lenis, et al., Expression of ABCA4 in the retinal pigment epithelium and its implications for Stargardt macular degeneration, Proc. Natl. Acad. Sci. U. S. A. 115 (47) (2018) E11120–E11127.
[5] M. Illing, L.L. Molday, R.S. Molday, The 220-kDa rim protein of retinal rod outer segments is a member of the ABC transporter superfamily, J. Biol. Chem. 272 (15) (1997) 10303–10310.
[6] A.V. Cideciyan, et al., Mutations in ABCA4 result in accumulation of lipofuscin before slowing of the retinoid cycle: a reappraisal of the human disease sequence, Hum. Mol. Genet. 13 (5) (2004) 525–534.
[7] F.C. Delori, et al., In vivo measurement of lipofuscin in Stargardt's disease–Fundus flavimaculatus, Invest. Ophthalmol. Vis. Sci. 36 (11) (1995) 2327–2331.
[8] R.A. Radu, et al., Complement system dysregulation and inflammation in the retinal pigment epithelium of a mouse model for Stargardt macular degeneration, J. Biol. Chem. 286 (21) (2011) 18593–18601.
[9] N.L. Mata, J. Weng, G.H. Travis, Biosynthesis of a major lipofuscin fluorophore in mice and humans with ABCR-mediated retinal and macular degeneration, Proc. Natl. Acad. Sci. U. S. A. 97 (13) (2000) 7154–7159.
[10] S. De, T.P. Sakmar, Interaction of A2E with model membranes. Implications to the pathogenesis of age-related macular degeneration, J. Gen. Physiol. 120 (2) (2002) 147–157.
[11] S.C. Finnemann, L.W. Leung, E. Rodriguez-Boulan, The lipofuscin component A2E selectively inhibits phagolysosomal degradation of photoreceptor phospholipid by the retinal pigment epithelium, Proc. Natl. Acad. Sci. U. S. A. 99 (6) (2002) 3842–3847.
[12] F. Schutt, et al., Photodamage to human RPE cells by A2-E, a retinoid component of lipofuscin, Invest. Ophthalmol. Vis. Sci. 41 (8) (2000) 2303–2308.
[13] J.R. Sparrow, K. Nakanishi, C.A. Parish, The lipofuscin fluorophore A2E mediates blue light-induced damage to retinal pigmented epithelial cells, Invest. Ophthalmol. Vis. Sci. 41 (7) (2000) 1981–1989.
[14] N.E. Fishkin, et al., Isolation and characterization of a retinal pigment epithelial cell fluorophore: an all-trans-retinal dimer conjugate, Proc. Natl. Acad. Sci. U. S. A. 102 (20) (2005) 7091–7096.
[15] J. Zhou, et al., Complement activation by photooxidation products of A2E, a lipofuscin constituent of the retinal pigment epithelium, Proc. Natl. Acad. Sci. U. S. A. 103 (44) (2006) 16182–16187.
[16] J. Zhou, et al., Complement activation by bisretinoid constituents of RPE lipofuscin, Invest. Ophthalmol. Vis. Sci. 50 (3) (2009) 1392–1399.
[17] R.A. Radu, et al., Bisretinoid-mediated complement activation on retinal pigment epithelial cells is dependent on complement factor H haplotype, J. Biol. Chem. 289 (13) (2014) 9113–9120.

[18] P. Yang, et al., Expression and modulation of RPE cell membrane complement regulatory proteins, Invest. Ophthalmol. Vis. Sci. 50 (7) (2009) 3473–3481.
[19] J.V. Sarma, P.A. Ward, The complement system, Cell Tissue Res. 343 (1) (2011) 227–235.
[20] A.O. Edwards, et al., Complement factor H polymorphism and age-related macular degeneration, Science 308 (5720) (2005) 421–424.
[21] G.S. Hageman, et al., A common haplotype in the complement regulatory gene factor H (HF1/CFH) predisposes individuals to age-related macular degeneration, Proc. Natl. Acad. Sci. U. S. A. 102 (20) (2005) 7227–7232.
[22] J.L. Haines, et al., Complement factor H variant increases the risk of age-related macular degeneration, Science 308 (5720) (2005) 419–421.
[23] R.J. Klein, et al., Complement factor H polymorphism in age-related macular degeneration, Science 308 (5720) (2005) 385–389.
[24] R. Klein, et al., Risk alleles in CFH and ARMS2 and the long-term natural history of age-related macular degeneration: the Beaver Dam Eye Study, JAMA. Ophthalmol. 131 (3) (2013) 383–392.
[25] M. Ansari, et al., Genetic influences on plasma CFH and CFHR1 concentrations and their role in susceptibility to age-related macular degeneration, Hum. Mol. Genet. 22 (23) (2013) 4857–4869.
[26] B.S. Blaum, et al., Structural basis for sialic acid-mediated self-recognition by complement factor H, Nat. Chem. Biol. 11 (1) (2015) 77–82.
[27] D.H. Anderson, et al., A role for local inflammation in the formation of drusen in the aging eye, Am. J. Ophthalmol. 134 (3) (2002) 411–431.
[28] V.L. Bonilha, et al., Geographic atrophy: confocal scanning laser ophthalmoscopy, histology, and inflammation in the region of expanding lesions, Invest. Ophthalmol. Vis. Sci. 61 (8) (2020) 15.
[29] J.W. Crabb, et al., Drusen proteome analysis: an approach to the etiology of age-related macular degeneration, Proc. Natl. Acad. Sci. U. S. A. 99 (23) (2002) 14682–14687.
[30] G.S. Hageman, et al., An integrated hypothesis that considers drusen as biomarkers of immune-mediated processes at the RPE-Bruch's membrane interface in aging and age-related macular degeneration, Prog. Retin. Eye Res. 20 (6) (2001) 705–732.
[31] R.F. Mullins, et al., Drusen associated with aging and age-related macular degeneration contain proteins common to extracellular deposits associated with atherosclerosis, elastosis, amyloidosis, and dense deposit disease, Faseb. J. 14 (7) (2000) 835–846.
[32] T.L. Lenis, et al., Complement modulation in the retinal pigment epithelium rescues photoreceptor degeneration in a mouse model of Stargardt disease, Proc. Natl. Acad. Sci. U. S. A. 114 (15) (2017) 3987–3992.
[33] V.L. Bonilha, et al., Retinal deimination and PAD2 levels in retinas from donors with age-related macular degeneration (AMD), Exp. Eye Res. 111 (2013) 71–78.
[34] V.L. Bonilha, et al., Retinal histopathology in eyes from a patient with Stargardt disease caused by compound heterozygous ABCA4 mutations, Ophthalmic Genet. 37 (2) (2016) 150–160.
[35] M.M. Edwards, et al., Retinal glial and choroidal vascular pathology in donors clinically diagnosed with Stargardt disease, Invest. Ophthalmol. Vis. Sci. 61 (8) (2020) 27.
[36] C.D. Birnbach, et al., Histopathology and immunocytochemistry of the neurosensory retina in fundus flavimaculatus, Ophthalmology 101 (7) (1994) 1211–1219.
[37] T. Taubitz, et al., Ultrastructural alterations in the retinal pigment epithelium and photoreceptors of a Stargardt patient and three Stargardt mouse models: indication for the central role of RPE melanin in oxidative stress, PeerJ 6 (2018) e5215.
[38] M.F. Abalem, et al., Peripheral visual fields in ABCA4 Stargardt disease and correlation with disease extent on ultra-widefield fundus autofluorescence, Am. J. Ophthalmol. 184 (2017) 181–188.
[39] M. Georgiou, et al., Prospective cohort study of childhood-onset Stargardt disease: fundus autofluorescence imaging, progression, comparison with adult-onset disease, and disease symmetry, Am. J. Ophthalmol. 211 (2020) 159–175.
[40] R. Allikmets, et al., Mutation of the Stargardt disease gene (ABCR) in age-related macular degeneration, Science 277 (5333) (1997) 1805–1807.
[41] L. Ciccone, et al., Hyperreflective deposition in the background of advanced Stargardt disease, Retina 38 (11) (2018) 2214–2219.
[42] S.S. Cornelis, et al., *In* silico functional meta-analysis of 5,962 ABCA4 variants in 3,928 retinal dystrophy cases, Hum. Mutat. 38 (4) (2017) 400–408.
[43] L.G. Fritsche, et al., A subgroup of age-related macular degeneration is associated with mono-allelic sequence variants in the ABCA4 gene, Invest. Ophthalmol. Vis. Sci. 53 (4) (2012) 2112–2118.
[44] J.R. Sparrow, M. Boulton, RPE lipofuscin and its role in retinal pathobiology, Exp. Eye Res. 80 (5) (2005) 595–606.
[45] J.R. Sparrow, D. Hicks, C.P. Hamel, The retinal pigment epithelium in health and disease, Curr. Mol. Med. 10 (9) (2010) 802–823.
[46] J.R. Sparrow, et al., Flecks in recessive Stargardt disease: short-wavelength Autofluorescence, near-infrared autofluorescence, and optical coherence tomography, Invest. Ophthalmol. Vis. Sci. 56 (8) (2015) 5029–5039.
[47] J.R. Sparrow, Quantitative fundus autofluorescence, JAMA. Ophthalmol. 135 (4) (2017) 403.
[48] J.R. Sparrow, et al., The bisretinoids of retinal pigment epithelium, Prog. Retin. Eye Res. 31 (2) (2012) 121–135.
[49] C.J. Boon, et al., Clinical and molecular genetic analysis of best vitelliform macular dystrophy, Retina 29 (6) (2009) 835–847.
[50] C.J. Boon, et al., Mutations in the peripherin/RDS gene are an important cause of multifocal pattern dystrophy simulating STGD1/fundus flavimaculatus, Br. J. Ophthalmol. 91 (11) (2007) 1504–1511.
[51] P.J. Guillausseau, et al., Maternally inherited diabetes and deafness: a multicenter study, Ann. Intern. Med. 134 (9 Pt 1) (2001) 721–728.
[52] C.J. Boon, et al., The spectrum of retinal dystrophies caused by mutations in the peripherin/RDS gene, Prog. Retin. Eye Res. 27 (2) (2008) 213–235.
[53] M. Michaelides, et al., Cone-rod dystrophy, intrafamilial variability, and incomplete penetrance associated with the R172W mutation in the peripherin/RDS gene, Ophthalmology 112 (9) (2005) 1592–1598.
[54] R. Riveiro-Alvarez, et al., New mutations in the RAB28 gene in 2 Spanish families with cone-rod dystrophy, JAMA. Ophthalmol. 133 (2) (2015) 133–139.
[55] S.H. Tsang, et al., Whole exome sequencing identifies CRB1 defect in an unusual maculopathy phenotype, Ophthalmology 121 (9) (2014) 1773–1782.
[56] J. Yang, et al., Validation of genome-wide association study (GWAS)-identified disease risk alleles with patient-specific stem cell lines, Hum. Mol. Genet. 23 (13) (2014) 3445–3455.
[57] J. Zernant, et al., Frequent hypomorphic alleles account for a significant fraction of ABCA4 disease and distinguish it from age-related macular degeneration, J. Med. Genet. 54 (6) (2017) 404–412.
[58] N.S. Bora, et al., Relationship between the complement system, risk factors and prediction models in age-related macular degeneration, Mol. Immunol. 63 (2) (2015) 176–183.
[59] S. McHarg, et al., Age-related macular degeneration and the role of the complement system, Mol. Immunol. 67 (1) (2015) 43–50.
[60] D.H. Anderson, et al., The pivotal role of the complement system in aging and age-related macular degeneration: hypothesis re-visited, Prog. Retin. Eye Res. 29 (2) (2010) 95–112.
[61] A. Georgiannakis, et al., Retinal pigment epithelial cells mitigate the effects of complement attack by endocytosis of C5b-9, J. Immunol. 195 (7) (2015) 3382–3389.
[62] R.F. Mullins, et al., Autosomal recessive retinitis pigmentosa due to ABCA4 mutations: clinical, pathologic, and molecular characterization, Invest. Ophthalmol. Vis. Sci. 53 (4) (2012) 1883–1894.
[63] D. Weismann, et al., Complement factor H binds malondialdehyde epitopes and protects from oxidative stress, Nature 478 (7367) (2011) 76–81.
[64] E. Kassa, et al., Complement inhibition as a therapeutic strategy in retinal disorders, Expet Opin. Biol. Ther. 19 (4) (2019) 335–342.